

DTIC FILE COPY

4

ARL-AERO-R-171

AR-004-496

AD-A200 516



DEPARTMENT OF DEFENCE
DEFENCE SCIENCE AND TECHNOLOGY ORGANISATION
AERONAUTICAL RESEARCH LABORATORIES
MELBOURNE, VICTORIA

Aerodynamics Report 171

DESIGN OF A NEW CONTRACTION FOR THE ARL
LOW SPEED WIND TUNNEL (U)

DTIC
ELECTE
NOV 09 1988
S D

by
J.H. WATMUFF

Approved for Public Release



(C) COMMONWEALTH OF AUSTRALIA 1986

88 11 09 04A

AUGUST 1984

DEPARTMENT OF DEFENCE
DEFENCE SCIENCE AND TECHNOLOGY ORGANISATION
AERONAUTICAL RESEARCH LABORATORIES

Aerodynamics Report 171

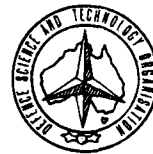
DESIGN OF A NEW CONTRACTION FOR THE ARL
LOW SPEED WIND TUNNEL (U)

by

J.H. Watmuff

SUMMARY

A numerical method is developed for the solution of Stokes's stream function. The method is applied to the existing Low Speed Wind Tunnel (LSWT) contraction shape. The calculated wall pressure coefficient distribution is compared to experimental measurements to test the approximation of axial symmetry made for the octagonal sections and for the effects of neglecting viscous forces. Reasonable agreement is obtained. The existing contraction is known to suffer from intermittent boundary layer separation near the entry caused by adverse pressure gradients. A new contraction shape is suggested that uses the contraction ratio of the existing LSWT so that the new design can be installed within the existing LSWT in the form of an inner skin. The new design, which is about 10% longer than the existing contraction, has an adverse pressure gradient near the inlet which is about 1/5 of that of the existing contraction while the adverse pressure gradient near the exit is around the same value. It is expected that the reduced adverse pressure gradient near the entry will be small enough to allow the inlet boundary layer to remain attached thus leading to a substantial improvement to the working section flow quality. The new design could be installed upstream of the existing contraction to provide increased working section length.



(C) COMMONWEALTH OF AUSTRALIA 1986

POSTAL ADDRESS: Director, Aeronautical Research Laboratories,
P.O. Box 4331, Melbourne, Victoria, 3001, Australia

1. INTRODUCTION

The acceleration of the flow in a wind tunnel contraction prior to the working section ensures that the rest of the tunnel circuit is subject to reduced losses in the tunnel wall boundary layers, turning vanes, screens and honeycomb. Mean-flow non-uniformities are reduced so that a more uniform velocity profile is obtained in the working section. The streamwise turbulence intensity in the working section is also reduced by stretching of the wakes from the turning vanes, honeycomb and screens.

Since the flow is accelerated by the contraction the pressure gradients on the walls are generally favourable. However it can be shown that for a finite length contraction two regions of adverse pressure gradient exist on the walls in the vicinity of the entrance and the exit. The presence of the contraction causes curvature of the streamlines in the upstream section of constant cross-sectional area causing the velocity to fall near the wall. The wall pressure continues to rise and reaches a local maximum near the inlet (but within the contraction) before beginning to fall. Similarly a pressure minimum (undershoot) occurs on the wall near the exit of the contraction. *As a result the velocity profile across the exit plane of a contraction is non-uniform and in a short contraction the non-uniformity may be as high as 10%.* The wall velocities approach the mean value asymptotically so that a model under test in the working section should be placed some distance downstream from the contraction exit, i.e. the useful length of the working section is reduced. The two regions of adverse pressure gradient can have a further detrimental effect by causing large-scale intermittent boundary layer separation resulting in increased unsteadiness of the flow in the working section.

The ARL low speed wind tunnel (LSWT) has been in almost continuous operation since it was commissioned in 1941. Figure 1 is a sketch of the tunnel showing the important dimensions. The contraction is characterised by an initially rapid rate of contraction followed by a much more gradual variation near the exit. It appears that the designers were more concerned about boundary layer separation caused by adverse pressure gradients near the contraction exit rather than near the entry. Batchelor and Shaw (1944) found that the total head in the working section fluctuates by around 1% throughout the test section. Larger fluctuations of up to 10% were experienced near a fillet. Turbulence intensity

measurements by D.C. Collis and M.J. Williams in 1946 indicate that the streamwise turbulence intensity varies from 0.2 to 0.7% depending on the location in the working section. The numerical computations of Batchelor and Shaw indicate that a major source of the unsteadiness may be due to intermittent boundary layer separation near the entry of the contraction caused by adverse pressure gradients. It is now well known (see Bradshaw 1973) that boundary layers are more unstable over concave surfaces (e.g. near a contraction inlet), than those over convex surfaces (e.g. near a contraction exit). Recent wool tuft flow visualisation studies have confirmed that the boundary layers at the entry to the contraction suffer from intermittent separation. The present configuration of the LSWT also has an unusually short working section which has required testing to be performed in regions that may be too close to the contraction exit for adequate flow uniformity.

Until recently theoretical methods of contraction design were considered unsatisfactory and most designers relied heavily on empirical methods. The analytical methods produce series solutions which are of little practical use. Some of the series solutions are inappropriate since they are periodic along the contraction axis. Others require impractically long axial lengths to obtain satisfactory entry and exit conditions. More recently a number of numerical solutions have become available for guiding the designer. The advantage of using numerical methods is that solutions may be obtained for an arbitrary contraction shape. Recent studies have been made for families of contraction shapes that are specified by a simply polynomial relating the radius to axial distance (Morel 1975). However there has been little published experimental evidence to confirm the adequacy of these designs. Willis and Hunt (1982) suggested a new design for the LSWT where the contraction ratio was increased from 4:1 to 7:1. Implementation of their design would require major modifications to the steel shell of the LSWT which would be an expensive and time consuming task. In this report a numerical method is developed for solving Stokes's stream function. On the basis of results from the calculation method a new LSWT contraction design is suggested. The contraction ratio is 4:1 so that the new design could be installed within the existing LSWT steel shell.

2. GOVERNING DIFFERENTIAL EQUATION

The continuity equation in an incompressible axisymmetric flow is given by,

$$\frac{1}{r} \frac{\partial(rV)}{\partial r} + \frac{\partial U}{\partial x} = 0$$

where x and r are coordinates in the axial and radial directions and U and V are the respective fluid velocities.

This equation is satisfied by defining a stream function ψ such that

$$U = \frac{1}{r} \frac{\partial \psi}{\partial r} \quad \text{and} \quad V = -\frac{1}{r} \frac{\partial \psi}{\partial x}$$

For irrotational flow, $\frac{\partial V}{\partial x} - \frac{\partial U}{\partial r} = 0$

$$\text{so that, } \frac{\partial^2 \psi}{\partial x^2} - \frac{1}{r} \frac{\partial \psi}{\partial r} + \frac{\partial^2 \psi}{\partial r^2} = 0 \quad (1)$$

The stream function ψ satisfying this equation is known as Stokes's stream function. Suitable boundary conditions for contraction are :

(1) $\psi = 0$ along the axis.

(2) $\psi = \psi_w = \text{constant}$, along the boundary.

(3) $\psi = (r/r_w)^2 \psi_w$

across the entry to the region of constant cross-sectional area upstream of the contraction ($r_w = \text{radius of tunnel boundary}$). This gives $U = 2\psi_w/r_w^2 = \text{constant}$.

Provided that the length of the parallel-walled entry region is large enough then the radial velocity component will also be zero i.e. the entry flow will be uniform and parallel to the axis.

- (4) $\partial^2 \psi / \partial x^2 = 0$ across the exit of the region of constant cross-sectional area downstream of the contraction.

3. THEORETICAL METHODS OF CONTRACTION DESIGN

Most analytical methods for contraction design are considered inappropriate for practical use. By far the most common analytical technique has been the method of separation of variables of equation 1. Depending on the choice of separation constant three possible series solutions may be constructed. Each of these solutions suffers from serious shortcomings. The first type of solution is restricted to families of axial velocity distributions which permit analytical expression of their derivatives e.g. Tsien (1943), Szeniewski (1943) and more recently Cohen and Ritchie (1962). The major difficulty in applying this type of solution arises from the stringent requirements on the form of the axial velocity distribution. Barger and Bowen (1972) generalised the method to cater for a wider range of velocity distributions so that the method could be applied to a greater variety of duct shapes. Nevertheless their approach is restrictive in the sense that only a limited number of contraction shapes can be obtained from the solutions. The velocities at the entrance and the exit are neither uniform nor parallel and a rather long contraction is required to avoid a strong adverse pressure gradient at the entrance. The second type of solution is periodic in the streamwise direction. Thwaites (1946) obtained series solutions in terms of Bessel functions. Since equation (1) is elliptic the effect of periodic repetition of the contraction shape will produce a flow different to that obtained with upstream and downstream regions of constant area. It is possible to specify parallel entrance and exit flow but the velocity distributions will not be uniform. Alternatively a uniform velocity distribution may be specified but at the expense of parallel entry and exit flow. However it can be shown in general that the entrance and exit velocity distributions cannot be both uniform and parallel if the entrance and exit are a finite distance apart. The third type of solution is in the form of an a periodic (exponential) series which produces solutions for the contraction shape which are infinitely long. A practical design based on this type of solution would need to be truncated which may produce unknown and undesirable affects. Other techniques that have been tried include Whitehead and Wu (1951) who used an approximate method where the velocity potential and

stream function of a two dimensional contraction are used as independent variables and the equation for the Stokes's stream function is solved numerically. Smith and Wang (1944) used a distribution of singularities such as ring vortices, sources and sinks to design a family of contractions.

It is unfortunate that there has been little experimental confirmation of the adequacy of these analytical solutions. One exception is the work by Bossell (1969) who built a 16:1 contraction based on a periodic solution of Stoke's stream function. Unfortunately his apparatus was rather small (exit diameter of 150mm) so that the experimental velocity profiles were affected by boundary layers near the walls. Nevertheless it would appear that the other differences observed between his experimental and theoretical velocity profiles have to be attributed to the fact that the theoretical result is based on a periodic solution.

Faced with these uncertainties, many designers have merely sketched plausible shapes by eye or selected a contour used previously elsewhere and believed to be acceptable. While many of these contractions have proved to be satisfactory, the ability to consider a new design in terms of a theoretical model must be considered an advantage.

Batchelor and Shaw (1944) were among the first to apply numerical methods to examine the flow properties of an axisymmetric contraction. The laborious computations for the current LSWT contraction were performed by hand. As mentioned in the introduction the design is characterised by an initially rapid rate of contraction followed by a more gradual variation near the exit. The results of their computations led them to suspect that the inlet boundary layer of the LWST may suffer from intermittent boundary layer separation causing increased unsteadiness of the flow in the working section.

Morel (1975) carried out a study aimed at providing practical guidelines for the design of axisymmetric contractions. Contours formed by two polynomial arcs joined smoothly together at an inflection point were examined. Cubic polynomials were found to form the most suitable wall shape and these were selected for a detailed study. Finite-difference solutions of the Euler equations were used to produce design charts which define the contraction length and position of the inflection point in terms of allowable adverse pressure gradients at the inlet and the exit and the desired exit flow uniformity. Morel was the first to

show the remarkable fact that for fixed requirements, the contraction length decreases as the contraction ratio increases.

Mikhail (1979) proposed a method for the optimum design of a wind tunnel contraction defined to be the shortest one that avoids boundary layer separation and which supplies the flow to the working section with a specified uniformity. Boundary layer calculations were made using a computer program based on the 'lag-entrainment' method which takes into account the wall curvature. He showed that by optimising the contraction wall curvature it is possible to reduce the contraction length considerably. Turbulent flow separation was predicted using Stratford's criterion. The behaviour of turbulent boundary layers with extra strain rates (such as those caused by streamline curvature, streamline divergence or pressure gradients) is still the subject of current research. It is doubtful whether Stratford's criterion can be applied with any confidence to boundary layers on a contraction wall which experience streamline curvature, streamline convergence and pressure gradients. It is unfortunate that Mikhail has provided no experimental verification for his suggestions. Therefore the behaviour predicted by his study must be treated with caution.

Recently Downie, Jordinson and Barnes (1984) described a method for calculating incompressible inviscid flow through ducts of rectangular cross-section. The method is based on a finite difference numerical solution of Laplace's equation for the velocity potential in three dimensions. Downie et al compared the prediction of their numerical calculations with experimental measurements and found satisfactory agreement. The magnitudes of the pressure overshoots and undershoots were found to be smaller in the experiments presumably because of the cushioning effects of boundary layer thickening. An interesting aspect of their work is the plotting of contours of the pressure coefficient distribution superimposed on the sides of the contraction walls (see their figure 6). These results have certain implications regarding the approximation of axial symmetry as applied to ducts of octagonal cross-section. For ducts of rectangular cross-section they found that the regions of pressure overshoot and undershoot are characterised by closed contours located near the contractions entry and exit planes and which are centred on the duct corners. It is likely that in an octagonal-sectioned contraction similar overshoots and undershoots of the pressure coefficient would occur at the corners and these would be larger than those seen along the wall centrelines. Since an octagonal

section is a better approximation to a circular section, than is a rectangular section, and since the effects of boundary layers in a real contraction appear to reduce the pressure overshoots and undershoots, it seems reasonable to approximate an octagonal section with axial symmetry.

4. EXPERIMENTAL VERIFICATION OF NUMERICAL METHOD

A numerical method has been developed for the solution for Stokes's stream function (i.e. equation 1) with the prescribed boundary conditions. Since the equation is elliptic the solution is affected by upstream and downstream conditions so the computational domain is fitted with parallel-walled extensions to the contraction inlet and outlet that are both 0.225 inlet diameters long. The numerical techniques are described in detail in Appendix A. Values of the streamwise velocity U and the radial velocity V are obtained by differentiating cubic splines that are fitted to the solutions for the stream function at each grid point and to the boundary values. Pressure coefficients C_p based on the streamwise velocity at the most downstream point on the axis are calculated from the Bernoulli equation so that the variation of the C_p along the contraction walls may be examined. Contours of constant C_p can also be calculated.

To test the approximations of axial symmetry made for octagonal sections and for the effects of neglecting viscous forces, the pressure coefficient distribution for the existing LSWT contraction shape has been calculated for comparison with experimental measurements. The equivalent radius of the axisymmetric contraction was determined from the octagonal cross-sectional area at 12 axial positions. The dimensions of the octagonal sections were taken from a drawing which was used to construct a 1/3.44 scale model of the LSWT known as the Pilot tunnel. The calculated wall pressure coefficients, shown in figure 2, are characterised by an almost constant value of C_p from the beginning of the parallel-walled entry section ($C_p = 0.9375$) through to near the entry of the contraction where an abrupt change to a region of almost constant pressure gradient occurs for about 1/8 of the contraction length.

The pressure coefficient levels off to a maximum value of 0.966 before falling to a minimum value of -0.062 near the contraction exit. A short region of adverse pressure gradient follows the C_p minimum which is about twice the magnitude of the adverse pressure gradient near the inlet. The contours shown in figure 3

indicate that the influence of the contraction extends further upstream than downstream. At the end of the contraction the entry flow to the working section is uniform to within around $\pm 1\%$.

Experimental measurements of the wall C_p distribution have been made in the Pilot tunnel which differs from the LSWT in that it is of the open return type. The maximum working section velocity is around 20 m/s. Figure 4 is a sketch of the tunnel showing relevant dimensions. Unfortunately the entry flow is characterised by an unsteady vortex originating on the floor. An effort was made to reduce the strength of the vortex by raising the tunnel by 300mm and by moving the entrance away from a nearby wall. Another cause of flow problems is that the tunnel entrance and exit are located in different rooms which are connected by an opening through which the tunnel passes. The return flow to the entrance was made more uniform by doubling the area of the opening and by placing baffles at locations selected by trial and error. Observations of smoke released on the floor near the entrance indicated that the strength of the vortex had been reduced considerably. A weak vortex remained which appeared and disappeared sporadically.

Static pressure tapings were placed along the contraction walls at equal axial intervals. Five rows of 46 tapings each are located along the centrelines of the contraction top wall, fillet and side wall and along the two vertices between these three surfaces, within one quadrant of the octagonal section as shown in figure 5. All tapings are connected to 48 port solenoid-driven scanivalves which are driven under computer control. A Pitot-static tube is fitted in the working section to provide the reference static and total pressures. The results of the experimental C_p measurements are shown in figures 6(a) to (e). All distributions have the characteristic C_p overshoot near the contraction entrance and an undershoot near the exit. Slightly larger undershoots are observed for the corner distributions which may be due to the corner vortices. The distributions on the top and side walls and along corner A show small positive excursions after the expected undershoot near the contraction exit. These excursions may be due to small misalignments at the junction between the contraction and working section.

All the experimental measurements and the results of the numerical calculation are superimposed in figure 7. The agreement of the experimental

and numerical results is reasonable except for the distribution measured along the top wall. The top wall C_p distribution has the lowest values in the first half of the contraction while it has the highest values in the second half, yet the entrance and exit values are in agreement with the other distributions. These results may be due to large-scale geometrical inaccuracies in the contraction shape here or to the effect of the entry vortex. The distributions measured on the centrelines of the top, fillet and side walls have smaller C_p undershoots than that predicted by the numerical calculation. This is consistent with the results of Downie et al who found that the experimental overshoots and undershoots were less than those predicted presumably because of local boundary layer thickening. On the basis of the results presented here it appears that the approximation of circular symmetry for an octagonal-sectioned contraction is reasonable and that the numerical calculations for a new LSWT contraction shape will act as a satisfactory guide for predicting its performance.

5. SELECTION OF A NEW CONTRACTION SHAPE FOR THE LSWT

A reasonable criterion for the selection of a new contraction shape for the LSWT is to minimise the adverse pressure gradient near the inlet while not significantly increasing the adverse pressure gradient near the exit. A variety of contraction shapes can be specified by two simple polynomial arcs which are joined together at an inflection point (see Morel 1975). Using the notation of figure 8 then,

$$\text{for } 0 < x < X_1, \quad R = R_1 - A_1 x^n \quad 2(a)$$

$$\text{and for, } X_1 < x < L_c, \quad R = R_0 + A_2 [L_c - x]^n \quad 2(b)$$

where n is an exponent which controls the maximum steepness of the contraction shape. By matching the gradient of the arcs at the inflection point the constants A_1 and A_2 are given by,

$$A_1 = \frac{(R_1 - R_0)}{X_1^{n-1} L_c}, \quad A_2 = \frac{(R_1 - R_0)}{(L_c - X_1)^{n-1} L_c}$$

From intuition one would expect that the position and magnitude of the adverse pressure gradients near the inlet and outlet of a contraction to be related to the wall curvature distribution. Morel tested six power-law contraction curves of order $n = 2, 2.5, 3.0, 3.5,$ and 4.0 , all of which had the same contraction ratio (9:1), length to inlet diameter ratio ($L_c/D_i = 1$) and nondimensional distance from the inlet to the inflection point ($X=X_i/L_c=0.5$). As the exponent n is reduced the wall curvature near both the entry and the exit decreases so that the pressure extrema and adverse pressure gradients also may be expected to decrease. However Morel's computations indicate that this effect only occurs for exponents greater than 3.

To check that this surprising result also occurs for the contraction ratio of the LSWT the C_p distributions for the contraction curves given by $n = 2, 3, 4$ and 5 were calculated. All the contraction curves had the same nondimensional distance to the inflection point ($X = 0.6$) and length-to-inlet-diameter ratio of the LSWT ($L_c/D_i = 0.881$). The wall C_p distributions shown in figure 9 indicate that as the polynomial order is increased from 3 to 5 both the entry and exit C_p extrema and adverse pressure gradients increase. Although the C_p maximum is small for $n = 2$, the adverse pressure gradient is still relatively large. For $n = 2$ the C_p minimum near the exit is larger than for $n = 3$ and the adverse pressure gradient is larger than all the other contraction curves. The ratios of the adverse pressure gradients to those estimated from the LSWT contraction calculation are approximately 0.40, 0.25, 0.36 and 0.67 near the entry and 4.3, 2.3, 2.6 and 3.3 near the exit for the contraction shapes given by $n = 2, 3, 4$ and 5 respectively. The C_p contours for $n = 2, 3$ and 4 shown in figures 10(a) to (c) indicate that the upstream and downstream influences of the contraction become larger as n is reduced. In all cases the greatest proportion of the working section length is required on the axis for the velocities to rise to within about 1% of the downstream reference velocity. Less working section length is required for the velocity overshoot at the boundary to fall to within the same tolerance.

Compared to the existing LSWT contraction the third-order contraction shape has an inlet adverse pressure gradient which is smaller by a factor of 4 while the adverse pressure gradient near the exit is larger by a factor of 2.3. Also the favourable pressure gradient near the centre of the contraction is about twice that of the LSWT so that there is the possibility of boundary layer relaminarisation here. Since laminar layers are more prone to separate than are

turbulent layers, the increased adverse pressure gradient at the exit may introduce new problems. It appears that the cubic profile with $X = 0.6$ may produce too large a modification to the adverse pressure gradients. If the exponent n in equations 2(a) and (b) is held constant the effect of moving the inflection point towards the contraction entry would be to decrease the curvature near the exit and increase the curvature near the entry. Hence the C_p minimum and the adverse pressure gradient near the exit would decrease at the expense of increasing the C_p maximum and adverse pressure gradient near the entry. Therefore solutions were obtained for the cubic contraction shape with $X = 0.5$ and $L_c/D_i = 0.881$. Calculations were also performed for contraction shapes with $n = 2.5$ and $n = 2.75$ to further examine the curious affect noted earlier regarding the C_p near the exit for $n < 3$.

The wall C_p distributions are shown in figure 11. The adverse pressure gradients near the contraction exit are all of similar magnitude. However, the contraction shape given by $n = 3$ offers the smallest C_p undershoot and adverse pressure gradient near the exit. The contours for the case $n = 3$ are shown in figure 12 and indicate that the entry flow to the working section approaches uniformity more rapidly than the case where $n = 3$ and $X = 0.6$ (see figure 10b). As may be expected from the wall curvature distribution, the upstream influence of the contraction is greater for the case $X = 0.5$ than for $X = 0.6$. The entry/exit pressure gradients are approximately 0.38 and 1.65 times those calculated for the LSWT contraction.

It appears that to achieve the criterion stated earlier for a new LSWT contraction it is necessary to increase the contraction length. Modern contraction designs usually have a length to inlet diameter ratio around 1 (see Mikhail 1979). A longer contraction could easily be accommodated by the LSWT since it has a rather longer settling chamber. The calculated wall C_p distribution for the contraction shape specified by $n = 3$, $X = 0.5$ and $L_c/D_i = 1$ is shown in figure 13. The inlet and outlet pressure gradients are approximately 0.20 and 0.91 times those calculated for the LSWT contraction. This contraction satisfies the criterion of reducing the entry adverse pressure gradient (by a factor of 5) while not increasing the adverse pressure gradient near the exit. The pressure coefficient contours shown in figure 14 indicate that the upstream and downstream influence of this contraction shape is small. In particular the flow at the exit of the contraction is uniform to within around $\pm 1\%$.

6. CONCLUDING REMARKS

To avoid interference with the steel shell the new design would have to be fitted into the LSWT upstream of the existing contraction. The new contraction could be made in the form of a fibreglass covered plywood skin which is supported by timber beams with much of the material being pre-fabricated so that the installation would proceed quickly. The results of the calculations suggest that a much shorter settling section could be used without affecting the uniformity of the entry flow to the contraction (see figure A2). According to the computations the settling region could be reduced in length by as much as 10ft. ($\approx 3\text{m}$)

leaving room for a screen to be installed after the honeycomb. The suggested arrangement shown in figure 15 would provide an extra 8 ft. ($\approx 2.4\text{m}$) of working section.

ACKNOWLEDGEMENTS

The author would like to thank N. Pollock for suggesting the problem and for following the course of the results as they came to hand. B.D.Fairlie and J.Lopez also provided stimulating discussions and advice throughout the work.

REFERENCES

- Barger, R.L. and Bowen, J.T. 1972.** 'A generalised theory for the design of contraction cones and other low-speed ducts'. NASA TN D6962.
- Batchelor, G.K. and Shaw, F.S. 1944.** 'A consideration in the design of wind tunnel contractions.' Australian Council for Aeronautics report ACA-4.
- Bossel, H.H. 1969.** 'Computation of axisymmetric contractions.' AIAA Journal, 7, 2017.
- Bradshaw, P. 1973.** 'Effects of streamline curvature on turbulent flow.' AGARDograph 169.
- Cohen, M.J. and Ritchie, N.J.B. 1962.** 'Low speed three-dimensional contraction design.' J.Roy. Aero. Soc., 66, 231.
- Downie, J.H., Jordinson, R. and Barnes, F.H. 1984.** 'On the design of three-dimensional wind tunnel contractions'. Aeronautical Journal, 88, 287.
- Mikhail, M.N. 1979.** 'Optimum design of wind tunnel contractions'. AIAA Journal, 17, 471.
- Morel, T. 1975.** 'Comprehensive design of axisymmetric wind tunnel contractions'. Trans. ASME, J. Fluids Eng. 225.
- Smith, G.D. 1978.** 'Numerical solutions of partial differential equations : finite difference methods'. Second edition, Clarendon Press, Oxford.
- Smith, R.H. and Wang, C.T. 1944.** 'Contracting cones giving uniform throat speeds.' J. Aeronautical Sci. 11, 356.
- Szczeniowski, B. 1943.** 'Contraction cone for a wind tunnel.' J. Roy. Aero. Soc., 10, 311.
- Thwaites, B. 1946.** 'On the design of contractions for wind tunnels.' Aero. Res. Council R&M 2278.
- Tsien, H. 1943.** 'On the design of the contraction cone for a wind tunnel.' J. Roy. Aeronautical Sci., 10, 68.
- Whitehead, L.G., Wu, L.Y. and Waters, M.H.L. 1951.** 'Contracting duct of finite length.' J. Roy. Aero. Soc., 11, 254.
- Willis, J.B. and Hunt, L.A. 1982.** 'Design of a new contraction, wide angle diffuser and flow manipulators for the low speed wind tunnel.' ARL Aero. Tech. Memo. 340.

APPENDIX A NUMERICAL TECHNIQUES**A.1 Relaxation method for solution of Stokes's stream function.**

A calculation method has been developed by author for the solution of Stokes's Stream Function, i.e. equation (1). The code was written in FORTRAN 77 and was developed and run on a 16-bit PDP 11/23-PLUS microcomputer. The development of the code on the microcomputer allowed rapid turnaround time during the edit, compile, task-build and debug stages of program development without incurring the inconvenience of mainframe computing. One of the problems of using a 16-bit computer for numerical computations is the small maximum program size available (65,536 16-bit words) which is much less than the typical memory size available with these machines. In order to make use of extra memory PDP 11 FORTRAN 77 allows arrays to be declared as VIRTUAL meaning that array values are stored outside the 65K program boundary. Hence large arrays do not consume program space which can be used for extra computational code.

Integration of the governing differential equation with the prescribed boundary conditions is accomplished using a numerical method based on the calculus of finite differences known as the relaxation method. Details of the method can be found in undergraduate textbooks (e.g. Smith 1978). The computational grid is generated by dividing the rectangular region up into equal sized intervals in the axial and in the radial directions. Currently the maximum number of grid lines in either direction is one hundred giving a maximum number of nodal intersection points of 10,000. For all cases reported here equal numbers of grid lines are used in both the axial and radial directions. Since the axial length of the computational region is always larger than the radial height much finer grid resolution is obtained in the radial direction. The finer resolution in the radial direction is an advantage due to the larger gradients of the stream function experienced near the tunnel boundaries. No attempt was made to use a non-uniform grid to cope with the larger gradients of the stream function experienced near the tunnel walls, nor was a coordinate transformation utilised to make the calculation domain rectangular (e.g. Mikhail 1979) since the ratio of the inlet to outlet diameters is only 2:1. Initial values are assigned to the nodal points as,

$$\psi = (r/r_w)^2 \psi_w$$

These values are systematically adjusted to satisfy equation (1) and the boundary conditions in an iterative manner. Nodal points outside the tunnel boundary are not used in the computation. Figure A1 shows a grid region where the contraction boundary intersects the grid points at A and B. In this region the lengths, a, b, c and d are not equal. Referring to figure A1 it can be shown that,

$$\psi_0 = \frac{\frac{2}{a+c} \left\{ \frac{\psi_1}{b} + \frac{\psi_3}{d} \right\} + \frac{2}{b+d} \left\{ \frac{\psi_2}{b} + \frac{\psi_4}{d} \right\} - \frac{(d/b)\psi_2 - (b/d)\psi_4}{r(b+d)}}{\frac{2}{ac} + \frac{2}{bd} + \frac{b/d - d/b}{r(b+d)}} \quad (A1)$$

Further within the contraction at points A', B', C', and D' for example, the lengths a' and c' are equal, and b' and d' are equal so that the expression for ψ_0 above is simplified.

Each iteration consists of calculating the new estimate (ψ_0) for each nodal point, except those in the first and last columns, using the values from the preceding iteration. The values for the first column specify the uniform and parallel entry flow so that the values here are kept fixed. The values for the points on the last column are evaluated from the finite difference approximation to the boundary condition $\partial^2 \psi / \partial x^2 = 0$. The node with the maximum percentage change from the previously iterated value is stored during each new iteration cycle. The iteration process is halted when this maximum percentage change falls below a user specified value. For all the results presented here the iterations were continued until all nodal values remained unchanged from their previous value i.e. the results had converged to around 7 significant figures. Although less convergence could be tolerated the author did not wish to become involved with deciding what a lesser tolerable convergence level might be.

The input to the program is an ASCII data file containing pairs of values representing the axial and radial coordinates of the tunnel profile to be tested. The origin of these data pairs (whether scaled from a sketch or obtained from a specified function) does not matter so long as the radius is constant or decreasing with streamwise distance. It is the user's responsibility to include adequate entry/exit region lengths in the file. A cubic spline is fitted to these data

points. The grid is generated on a rectangular region of length equal to the axial distance between the first and last data pairs and of height 1.001 times the inlet radius. The multiplying factor (1.001) is used to ensure that the tunnel boundary falls wholly within the rectangular region and that the tunnel boundary values would fall slightly over and some slightly under a grid line causing computational difficulties. It was found that the total computational time varied approximately as N^3 (where N = the number of axial grid lines = the number of radial grid lines). After some initial trials it was found that $N = 60$ would give results of ample resolution. For $N = 60$ the computations take around 15 hours (i.e. an overnight run) performing around 4000 iterations. At the end of each run a data file is created for subsequent analysis.

A.2 Evaluation of wall pressure coefficients.

The stream function solutions are processed to produce a file of the wall pressure coefficients for each axial grid coordinate. A cubic spline is applied to the stream function solutions at each grid point and at the boundary along each column in succession. Values of U ($= 1/r \partial \psi / \partial r$) are found at the boundary from the derivation of the spline fit. Since the boundary is a streamline and its slope can be calculated from the splined values of the boundary shape, the radial velocity component can also be calculated at the boundary. The values of the pressure coefficient at each columnar grid boundary position are simply evaluated from the Bernoulli equation as,

$$C_p = 1 - (U_B^2 + V_B^2) / U_{REF}^2 \quad (A2)$$

where U_B and V_B are the streamwise and radial boundary velocity components and U_{REF} is the streamwise velocity of the most downstream axis grid point. Values of U are indeterminate on the axis (since $U = 1/r \partial \psi / \partial r = 0/0$). A fifth order least squares polynomial of best fit passing through the closest point to the axis is extrapolated to the axis to evaluate U_{REF} .

A.3 Contour plotting.

Contours of constant pressure coefficient are calculated using a second-order predictor-corrector scheme which requires evaluation of the streamwise and radial directional derivatives of surfaces describing the C_p distribution over each grid region. The C_p values are determined from the Bernoulli equation (using equation A2 with the same reference velocity but using each grid value of U and V instead of the boundary values). Internal values of U and columnar boundary values of U and V are determined using the same techniques as described earlier. Similarly, cubic splines are applied to the stream function along each row (excluding the axis) for internal values of V at each grid point and row boundary values of V and U (using the slope of the boundary). Axis values of V are zero by definition. Therefore values of U and V (and hence C_p) can be found at each grid point inside the contraction boundary and at the intersection of each column and row with the boundary.

Over each grid region through which the contour is plotted, a surface polynomial in x and r is used to describe the variation of C_p . It is essential for accurate contouring that each surface possess common boundaries with those of the four adjoining regions. These boundaries are the result of cubic splines applied along the appropriate rows and columns. Since cubic splines are used each of the common boundaries can be fitted exactly with a third order polynomial. By adding two fourth order terms, linear in x and r respectively, the requirements of the surface fit can be satisfied i.e.

$$\begin{aligned}
 C_p = & A_1 \\
 & + A_2x + A_3r \\
 & + A_4x^2 + A_5x r + A_6r^2 \\
 & + A_7x^3 + A_8x^2r + A_9x r^2 + A_{10}r^3 \\
 & + A_{11}x r^3 + A_{12}x^3 r
 \end{aligned} \tag{A3}$$

The 12 unknown coefficients $A_1 \dots A_{12}$ are evaluated from 12 equations formed from the following conditions : the surface must pass through the four vertices of

the grid (4 equations) and the first derivatives $\partial C_p / \partial x$ and $\partial C_p / \partial r$ at each of the vertices must be equal to that indicated by the cubic splines (8 equations). While there is continuity of the C_p values across each boundary, continuity of first derivatives cannot be guaranteed except at the corners. The 12 coefficients can be obtained by the inversion of a 12x12 matrix. When the contour moves into a new region a new set of 12 coefficients must be used. In order to save computation time a localised stretched coordinate system $x' r'$ is used the origin at the centre of the grid region so that the region boundaries line on the lines $x' = \pm 1, r' = \pm 1$. The results of the inversion of the 12x12 matrix below can be performed once and stored so that the contouring program can rapidly calculate the coefficients $A_1 \dots A_{12}$ for each new grid region as required.

$$\begin{bmatrix}
 1 & 1 & 1 & 1 & 1 & 1 & 1 & 1 & 1 & 1 & 1 & 1 \\
 1 & -1 & 1 & 1 & -1 & 1 & -1 & 1 & -1 & 1 & -1 & -1 \\
 1 & -1 & -1 & 1 & 1 & 1 & 1 & 1 & -1 & -1 & 1 & 1 \\
 1 & 1 & -1 & 1 & -1 & 1 & 1 & -1 & 1 & -1 & -1 & -1 \\
 0 & 1 & 0 & 2 & 1 & 0 & 3 & 2 & 1 & 0 & 3 & 1 \\
 0 & 1 & 0 & -2 & 1 & 0 & 3 & -2 & 1 & 0 & 3 & 1 \\
 0 & 1 & 0 & -2 & -1 & 0 & 3 & 2 & 1 & 0 & -3 & -1 \\
 0 & 1 & 0 & 2 & -1 & 0 & 3 & -2 & 1 & 0 & -3 & -1 \\
 0 & 0 & 1 & 0 & 1 & 2 & 0 & 1 & 2 & 3 & 1 & 3 \\
 0 & 0 & 1 & 0 & -1 & 2 & 0 & 1 & -2 & 3 & -1 & -3 \\
 0 & 0 & 1 & 0 & -1 & -2 & 0 & 1 & 2 & 3 & -1 & -3 \\
 0 & 0 & 1 & 0 & 1 & -2 & 0 & 1 & -2 & 3 & 1 & 4
 \end{bmatrix}
 \begin{bmatrix}
 A_1 \\
 A_2 \\
 A_3 \\
 A_4 \\
 A_5 \\
 A_6 \\
 A_7 \\
 A_8 \\
 A_9 \\
 A_{10} \\
 A_{11} \\
 A_{12}
 \end{bmatrix}
 =
 \begin{bmatrix}
 (C_p)_1 \\
 (C_p)_2 \\
 (C_p)_3 \\
 (C_p)_4 \\
 (\partial C_p / \partial x')_1 \\
 (\partial C_p / \partial x')_2 \\
 (\partial C_p / \partial x')_3 \\
 (\partial C_p / \partial x')_4 \\
 (\partial C_p / \partial r')_1 \\
 (\partial C_p / \partial r')_2 \\
 (\partial C_p / \partial r')_3 \\
 (\partial C_p / \partial r')_4
 \end{bmatrix}$$

Problems arise with the surface fitting technique since grid regions which are cut by the tunnel boundary require values and derivatives of C_p that are outside the boundary i.e. some form of extrapolation is required. Depending on the relative size of the axial and radial grid intervals and on the slope of the contraction wall, regions were found where points up to three radial grid intervals outside the boundary were required for the surface fitting. Fifth-order least squares polynomials passing through the boundary values are used to the extrapolation. Purely radial extrapolations are used where the boundary radius is

greater than 0.9 times the inlet radius or less than 1.1 times the exit radius. For extrapolation where the boundary radius falls within these limits, the points outside the boundary that directly influence the contours are calculated using both radial and streamwise extrapolations. The extrapolated values are averaged by weighting them with the distances from the grid point to the opposite boundary respectively. Fifth-order polynomials in the radial direction that pass through these weighted averaged points are used to extrapolate for the values of U and V at the remaining grid points. Values are required at these points so that the grid region boundary splines in the regions used for contouring are not adversely affected.

A.4 Selection of inlet and outlet extension lengths.

Since the governing equation is elliptic in nature the flow within the contraction is sensitive to the upstream and downstream flow conditions. Therefore it is important that the lengths of the straight-walled sections before and after the contraction are large enough that truncation beyond them has negligible influence on the results. Morel (1975) used inlet and outlet extensions that were 0.7 local diameters in length. He reports that further lengthening had no influence on his results but made no mention of the effects of shortening the extensions. A series of calculations have been made using equal inlet/outlet extensions of lengths 0.125, 0.225, 0.325 and 0.425 times the inlet diameter for the cubic contraction shape shown in figure 10(b). The C_p contours shown in figures A2(a) to (d) reveal that only the contours near the inlet and outlet of the contraction with the nondimensional inlet/outlet extension length of 0.125 are significantly affected. Differences between the contours for the other cases are undetectable. Therefore inlet/outlet extensions that are 0.225 inlet diameters long were used for all computations unless otherwise specified.

APPENDIX B EXPERIMENTAL MEASUREMENTS OF PRESSURE COEFFICIENT.

Pressure coefficients have been measured along the contraction walls of the Pilot (LSWT model) tunnel. Five rows of 46 static pressure tappings each are located along the centerlines of the contraction top wall, fillet and side walls and along the two vertices between these three surfaces, within one quadrant of the octagonal section as shown in figure 5. The tappings are positioned according to arc lengths which has been calculated from the contraction geometry. The

calculated arc lengths over the contraction length (around 1500mm) were found to be within $\pm 1\text{mm}$ of the measured values. Therefore the axial positions of the tapplings can be regarded as precise. All tapplings are connected to 48 port solenoid-driven scanivalves via plastic tubing. Only three scanivalves are used for simultaneous measurements throughout the experiments due to a lack of pressure transducers with a suitable range. The three external differential pressure transducers used are :

- (1) Setra model 236 with a range of 0.2 psi and full scale output of 5v.
- (2) Setra model 236 with a range of 0.5 psi and full scale output of 5v.
- (3) Furness FC 6124 with a range of 1.5 psi and full scale output of 1v.

The outputs of the transducers are suitably amplified before measurement. The two extra ports on each scanivalve are connected to total and static pressures of a Pitot-Static tube located in the working section. The static pressure from the Pitot-Static tube is also used as a reference pressure for the transducers. Transducer drift is monitored and corrected for during the experiments by connecting the reference pressure across each transducer. Since five groups of pressure tapplings are measured, each experimental run was performed by connecting sets of three and two groups of connectors to the scanivalves in succession.

The scanivalve solenoids are operated by a controller with two inputs, namely 'single step' and 'return to home.' The PDP 11/23-PLUS microcomputer is used to operate the controllers and to store the amplified transducer outputs via a data logger with the brand name of Dataporte. The Dataporte is a compact intelligent microprocessor-based data acquisition system which can be supervised by any computer with an RS232C serial interface. Amongst the features of the Dataporte are analog, digital, event and counter inputs, data storage and averaging, analog and digital outputs, temperature measurement and a real time clock. Up to 46 single-ended analog input channels can be connected with autoranging over three decades. The Dataporte is controlled by issuing simple abbreviated English-like commands. The maximum sampling rate is around 20 samples/sec so that the system is only suitable in applications requiring low sampling rates. One of the eight digital outputs is used to step the three scanivalve solenoids in parallel at a rate of about 3 steps/sec while another digital output is used to simultaneously step the scanivalves to the home position.

Electronic integration of the amplified pressure transducers can be used to obtain true mean values over time periods of up to three minutes in duration. For the results presented in this report an integration time period of 15 seconds was used. Two digital outputs of the Dataport are used to start and reset the integrators while one of the digital inputs is used to detect completion of the integration cycle. The integrated voltages are then returned to the computer for processing and storage.

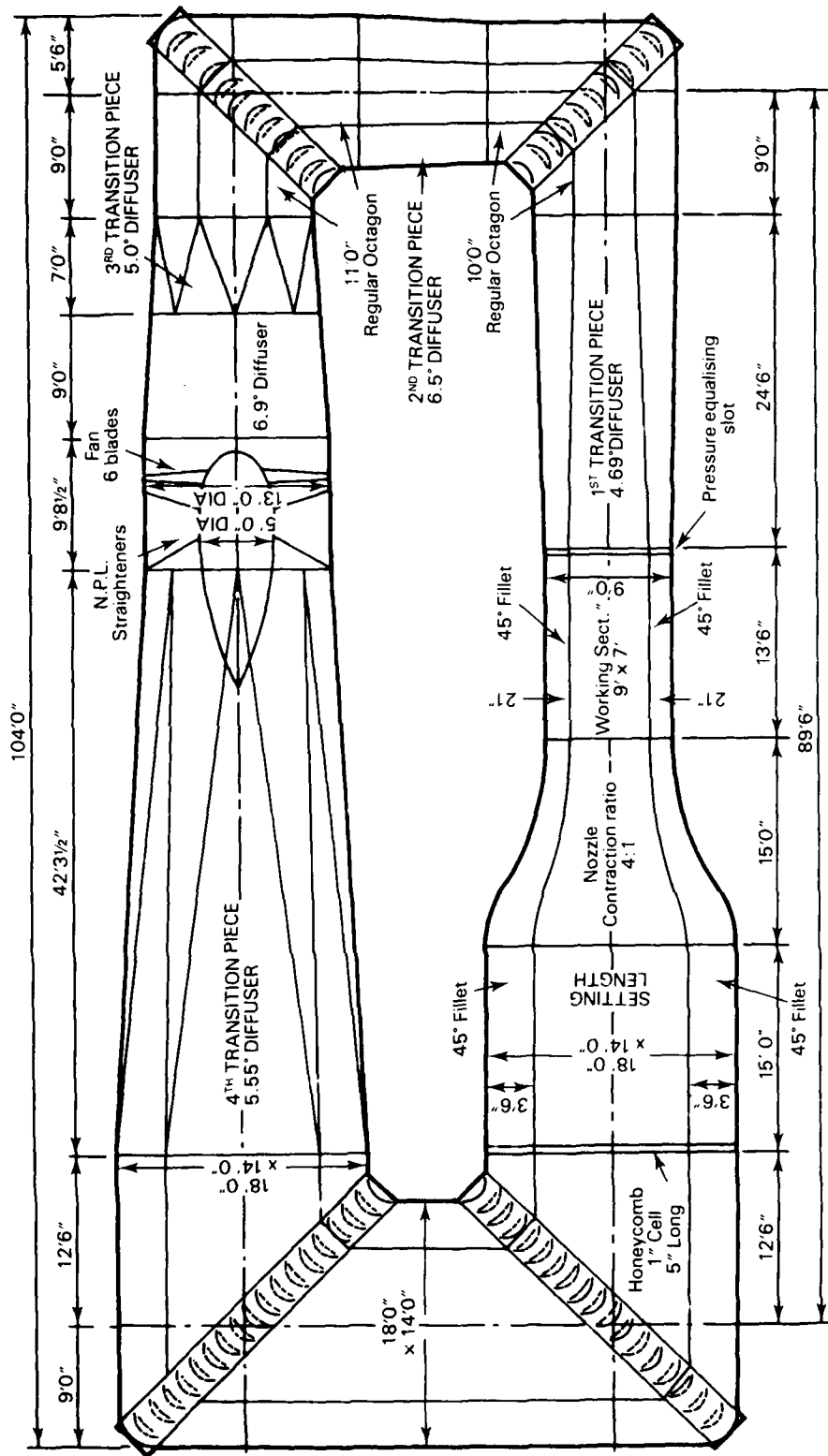


FIG. 1. SKETCH OF THE ARL LOW SPEED WIND TUNNEL (LSWT) SHOWING IMPORTANT DIMENSIONS.

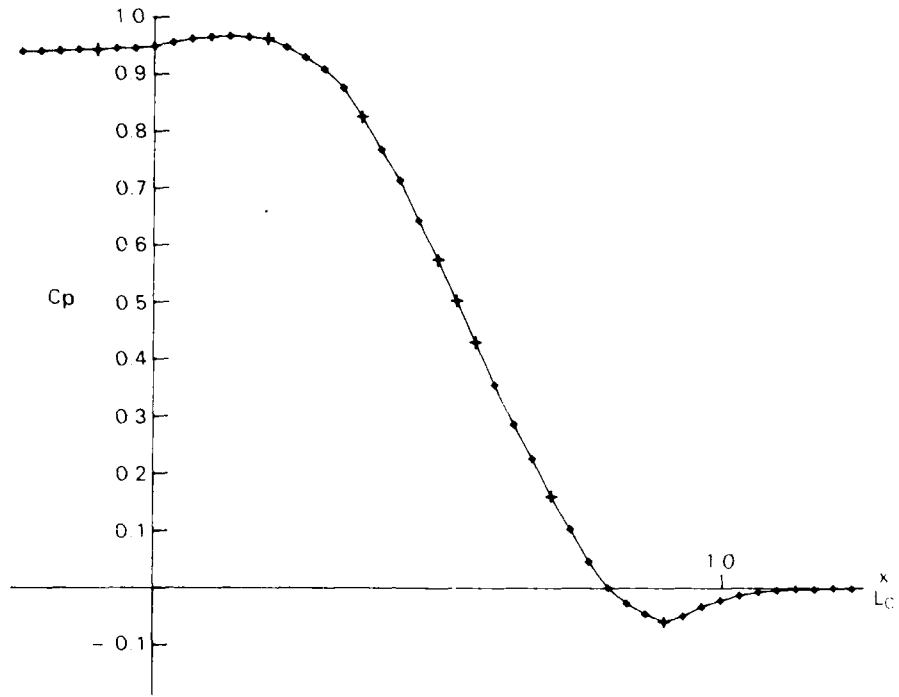


FIG. 2. CALCULATED WALL C_p DISTRIBUTION FOR THE EXISTING LSWT CONTRACTION.

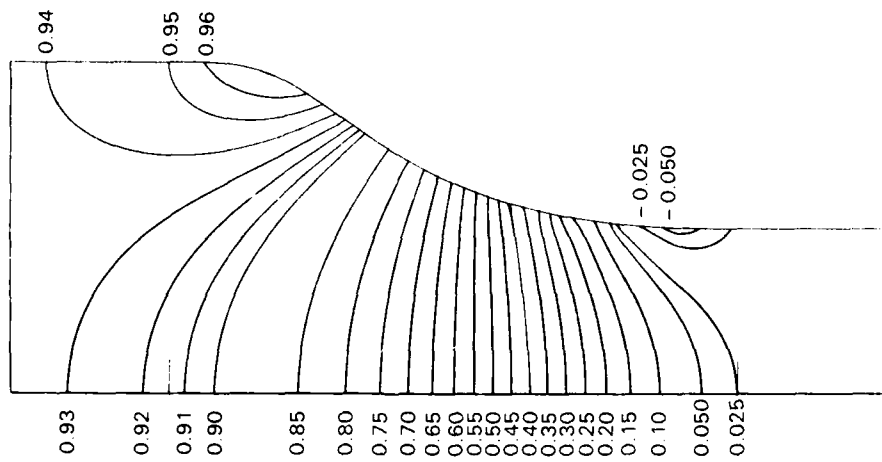


FIG. 3. CALCULATED CONTOURS OF C_p WITHIN THE LSWT.

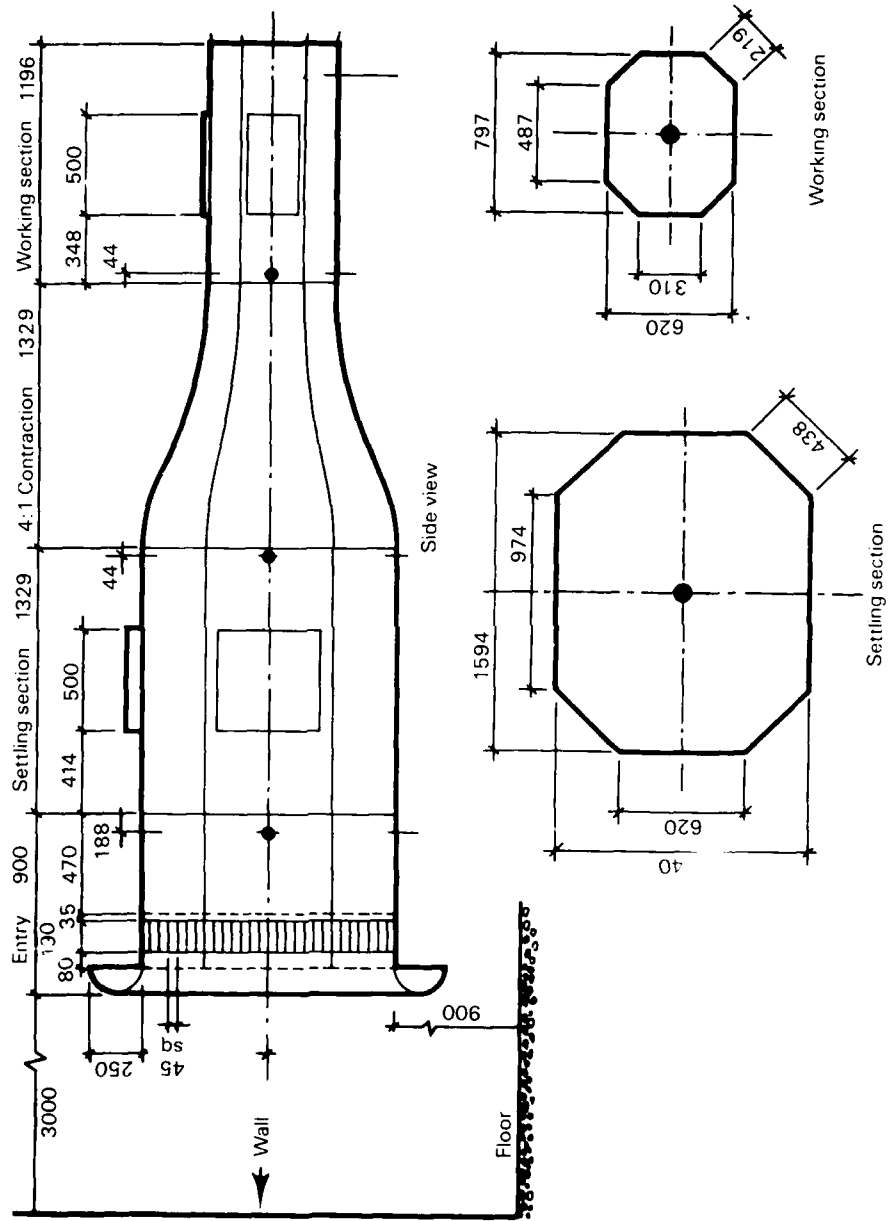


FIG. 4. SKETCH OF OPEN RETURN PILOT TUNNEL (LSWT MODEL) SHOWING RELEVANT DIMENSIONS.

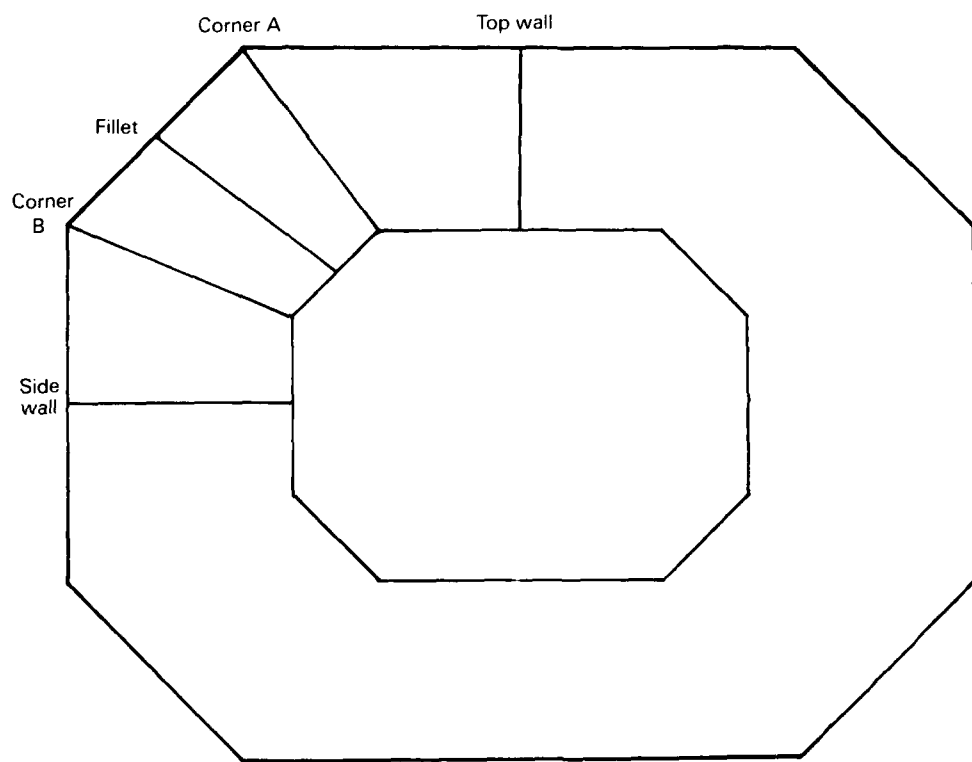


FIG. 5. LOCATIONS OF THE FIVE ROWS OF 46 PRESSURE TAPPINGS USED FOR THE EXPERIMENTAL C_p MEASUREMENTS IN THE PILOT TUNNEL.

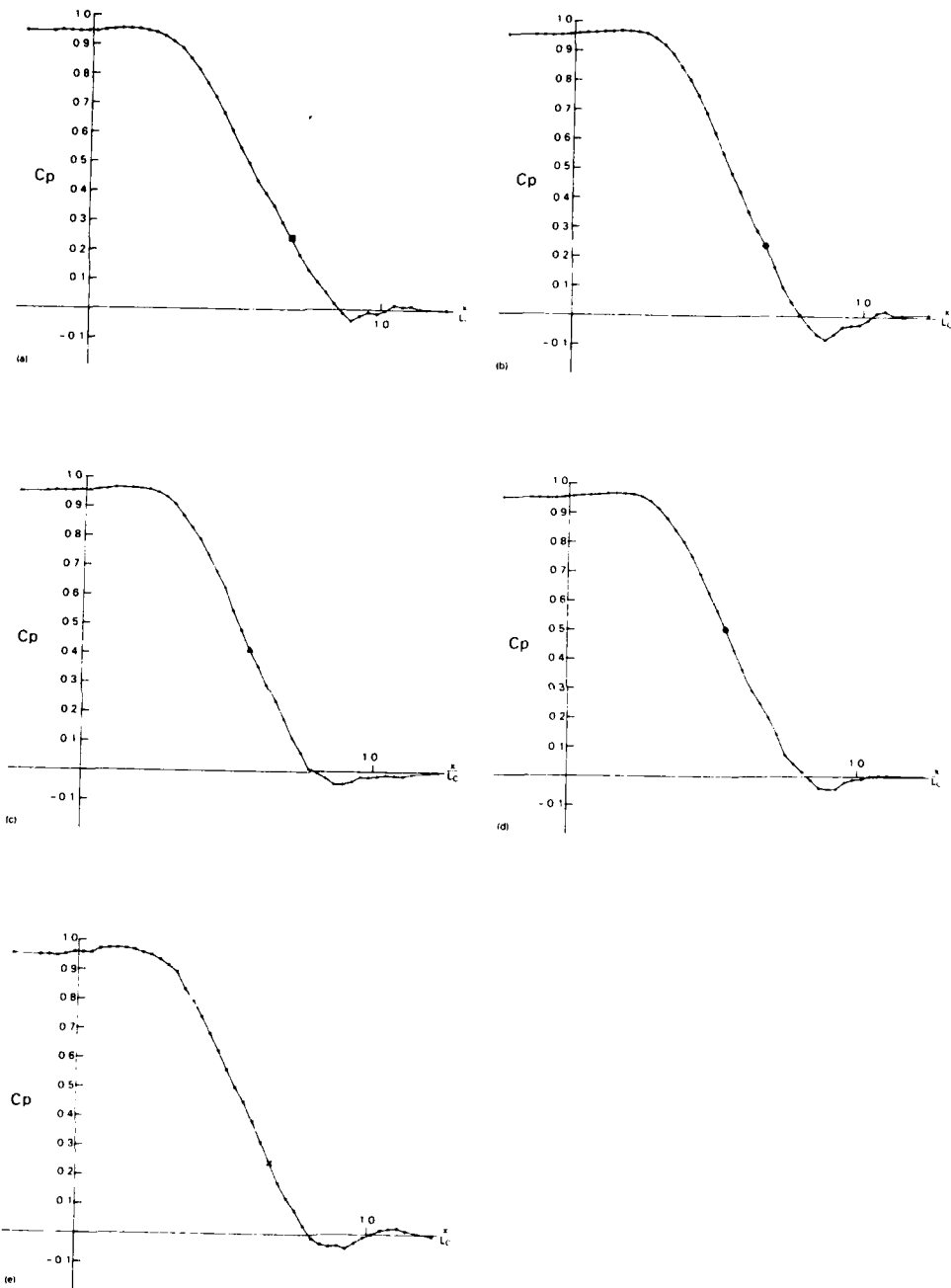


FIG. 6. EXPERIMENTAL MEASUREMENTS OF C_p ALONG (a) TOP WALL, (b) CORNER A, (c) FILLET, (d) CORNER B, (e) SIDE WALL.

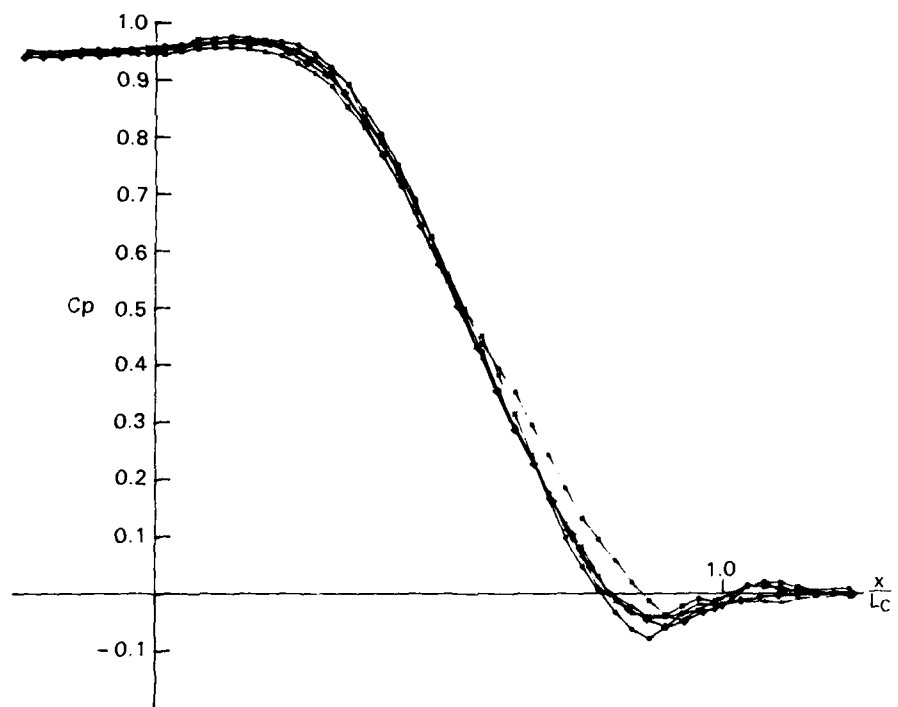


FIG. 7. CALCULATED AND EXPERIMENTAL VALUES OF C_p . SYMBOLS AS IN FIGS. 2 AND 6. EXCEPT FOR THE EXPERIMENTAL TOP WALL MEASUREMENTS, THE CALCULATED AND EXPERIMENTAL VALUES ARE IN REASONABLE AGREEMENT.

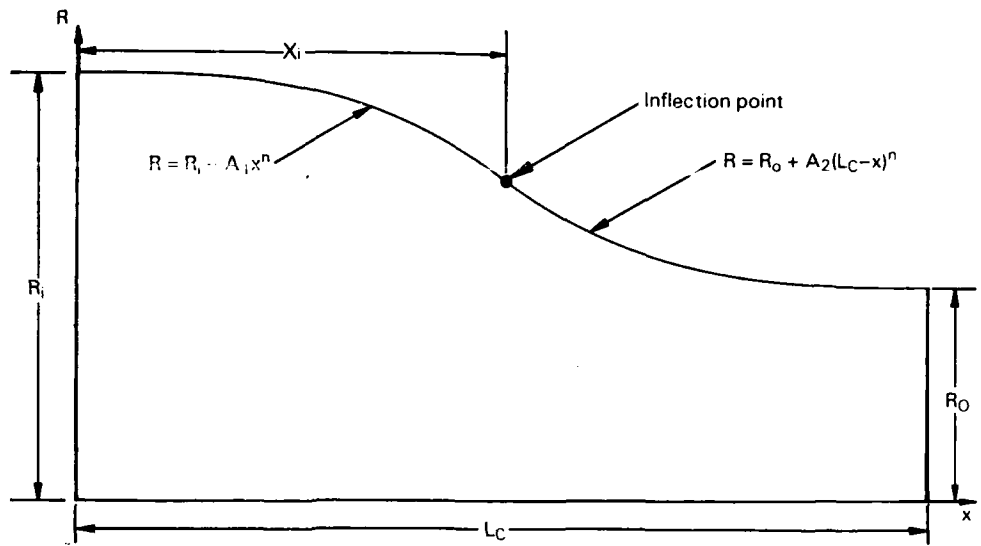


FIG. 8. NOTATION FOR CONTRACTION WALL CONTOUR CONSTRUCTED FROM TWO ARCS.

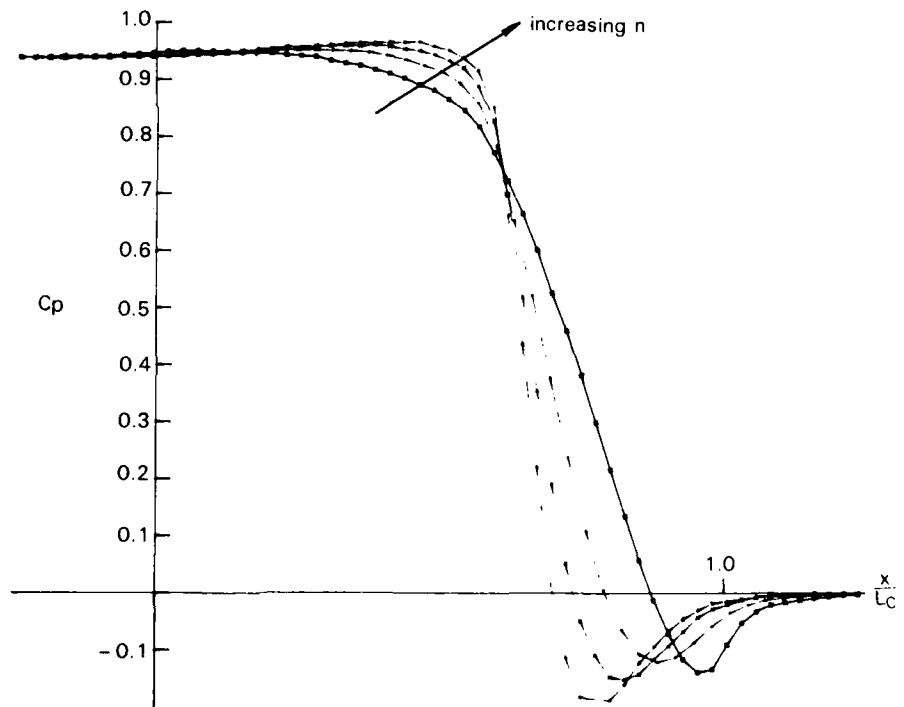


FIG. 9. CALCULATED WALL C_p DISTRIBUTIONS FOR $X=0.6$, $L_c/D_i=0.881$ (SAME AS LSWT) AND $n=2, 3, 4$ AND 5 . ARROW SHOWS ORDER OF INCREASING n .

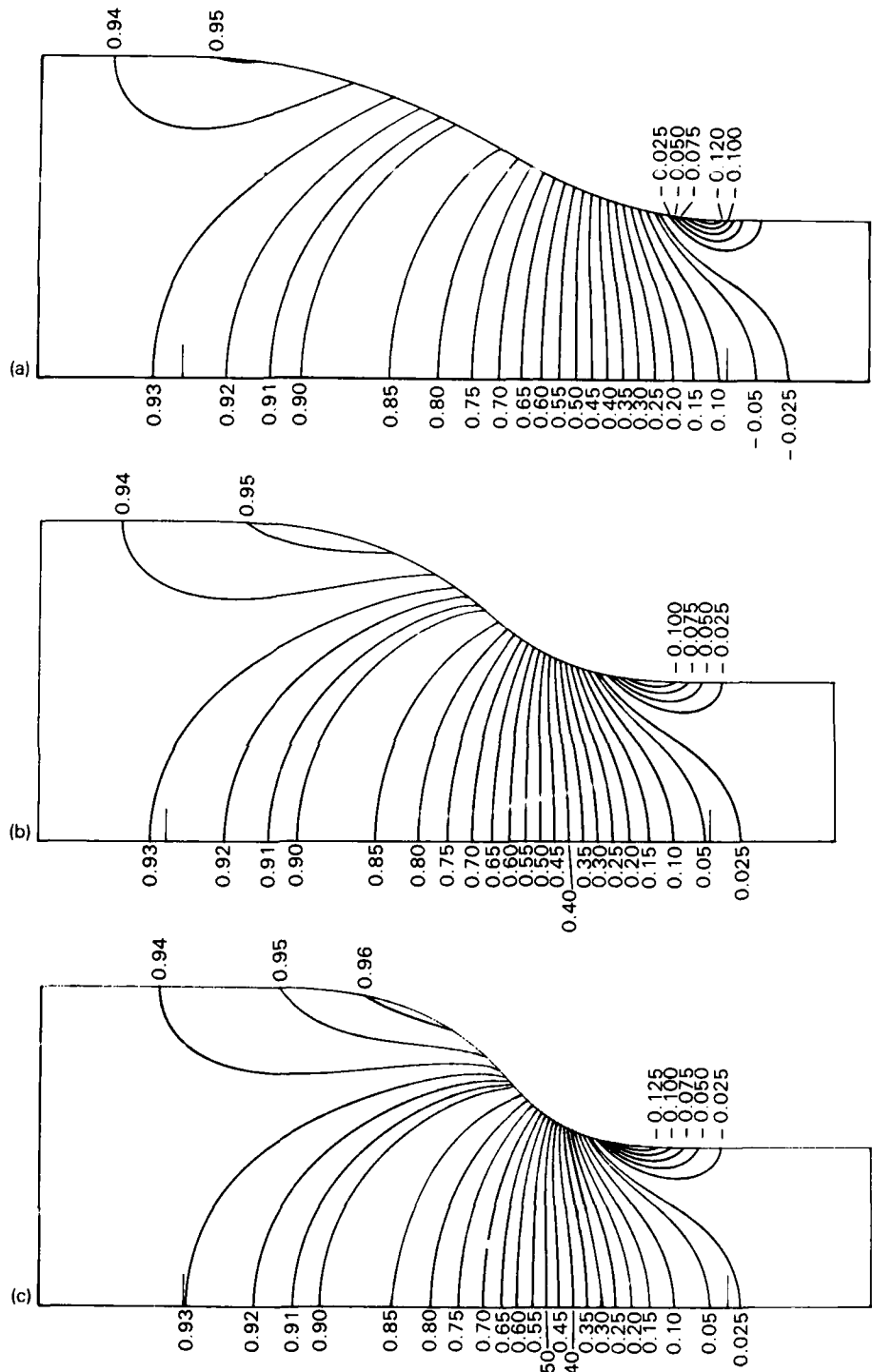


FIG. 10. CONTOURS OF C_p WITHIN CONTRACTIONS SPECIFIED IN FIG. 9. (a) $n=2$ (b) $n=3$ (c) $n=4$.

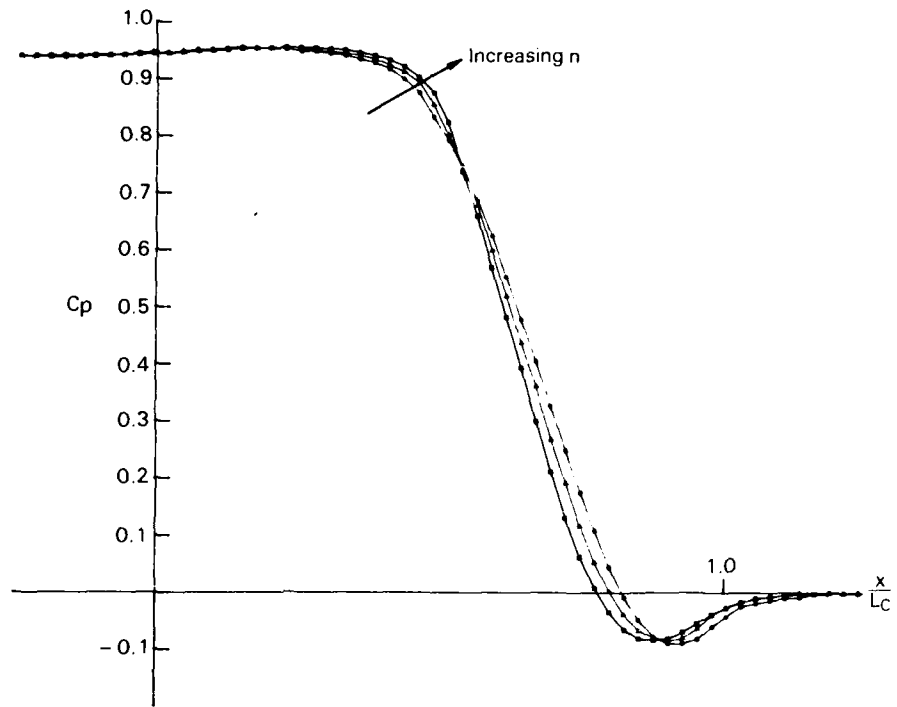


FIG. 11. CALCULATED WALL C_p DISTRIBUTIONS FOR $X=0.5$, $L_c/D_i=0.881$, AND $n=2.5, 2.75$ AND 3 . ARROW SHOWS ORDER OF INCREASING n .

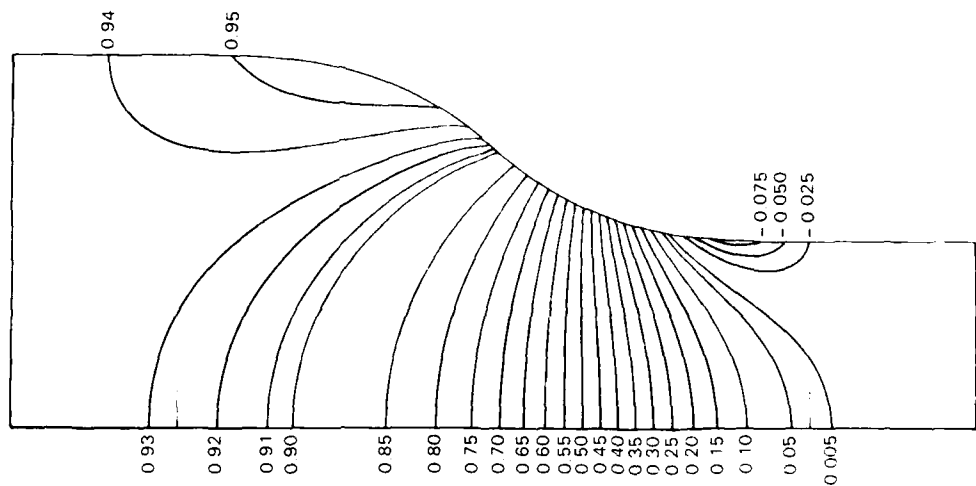


FIG. 12. CONTOURS OF C_p WITHIN CONTRACTION SPECIFIED IN FIG. 11 WITH $n=3$.

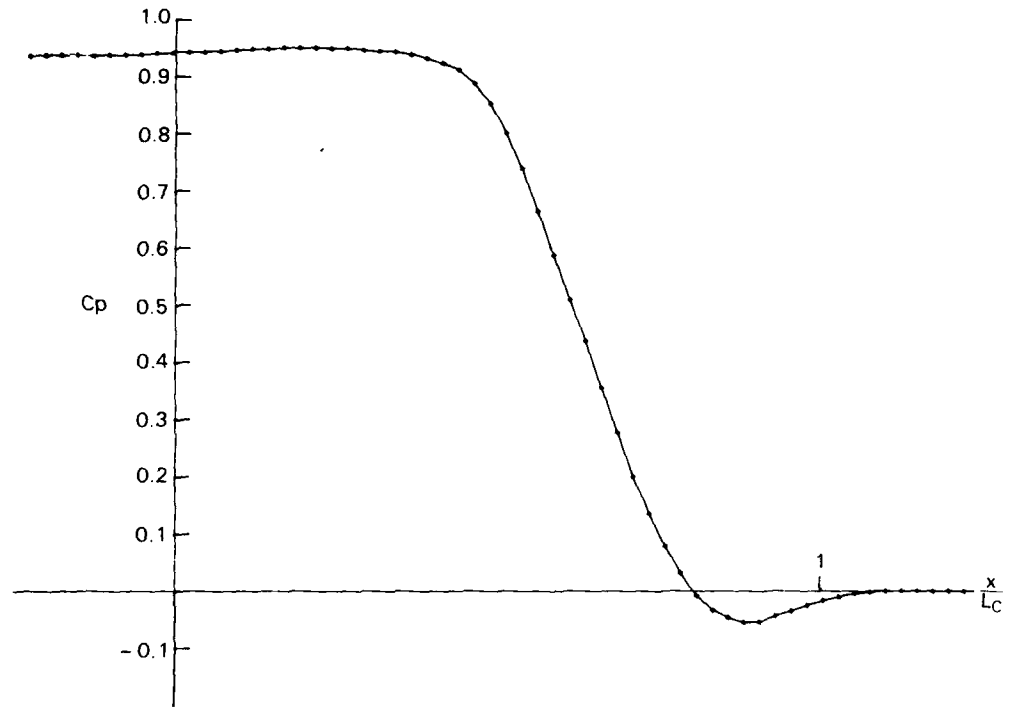


FIG. 13. CALCULATED WALL C_p DISTRIBUTION FOR $X=0.5$, $L_c/D_i=1$ AND $n=3$.

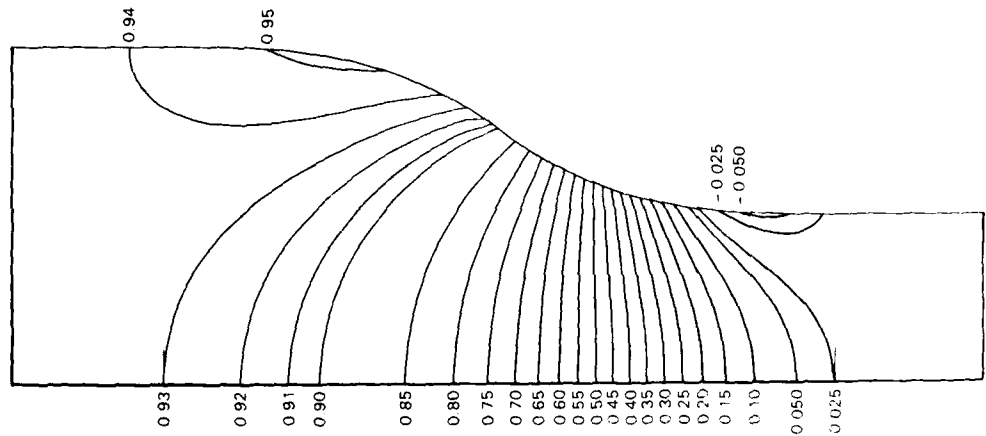


FIG. 14. CONTOURS OF C_p WITHIN CONTRACTION SPECIFIED IN FIG. 13. UNIFORMITY OF THE ENTRY FLOW TO THE WORKING SECTION IS SIMILAR TO LSWT CONTRACTION (SEE FIG. 3).

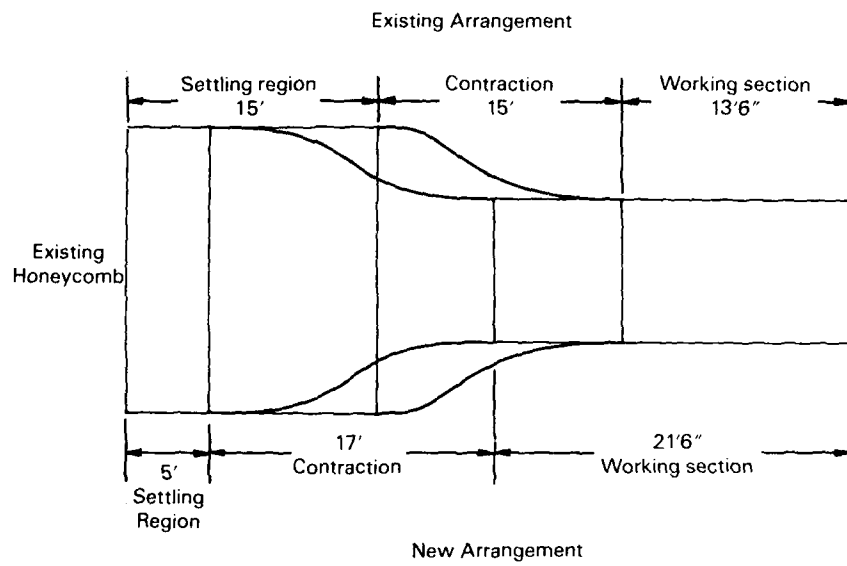


FIG. 15. SKETCH OF EXISTING SETTLING REGION, CONTRACTION, AND WORKING SECTION. SUGGESTED NEW ARRANGEMENT PROVIDING EXTRA 8 ft. (2.4m) OF WORKING SECTION ALSO SHOWN.

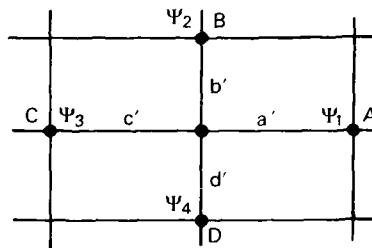
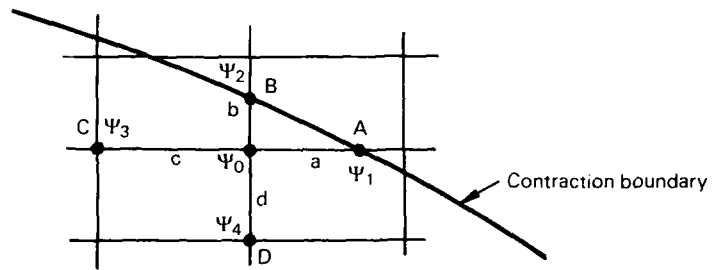


FIG. A1. NOTATION USED FOR STREAM FUNCTION CALCULATION GRID POINTS.

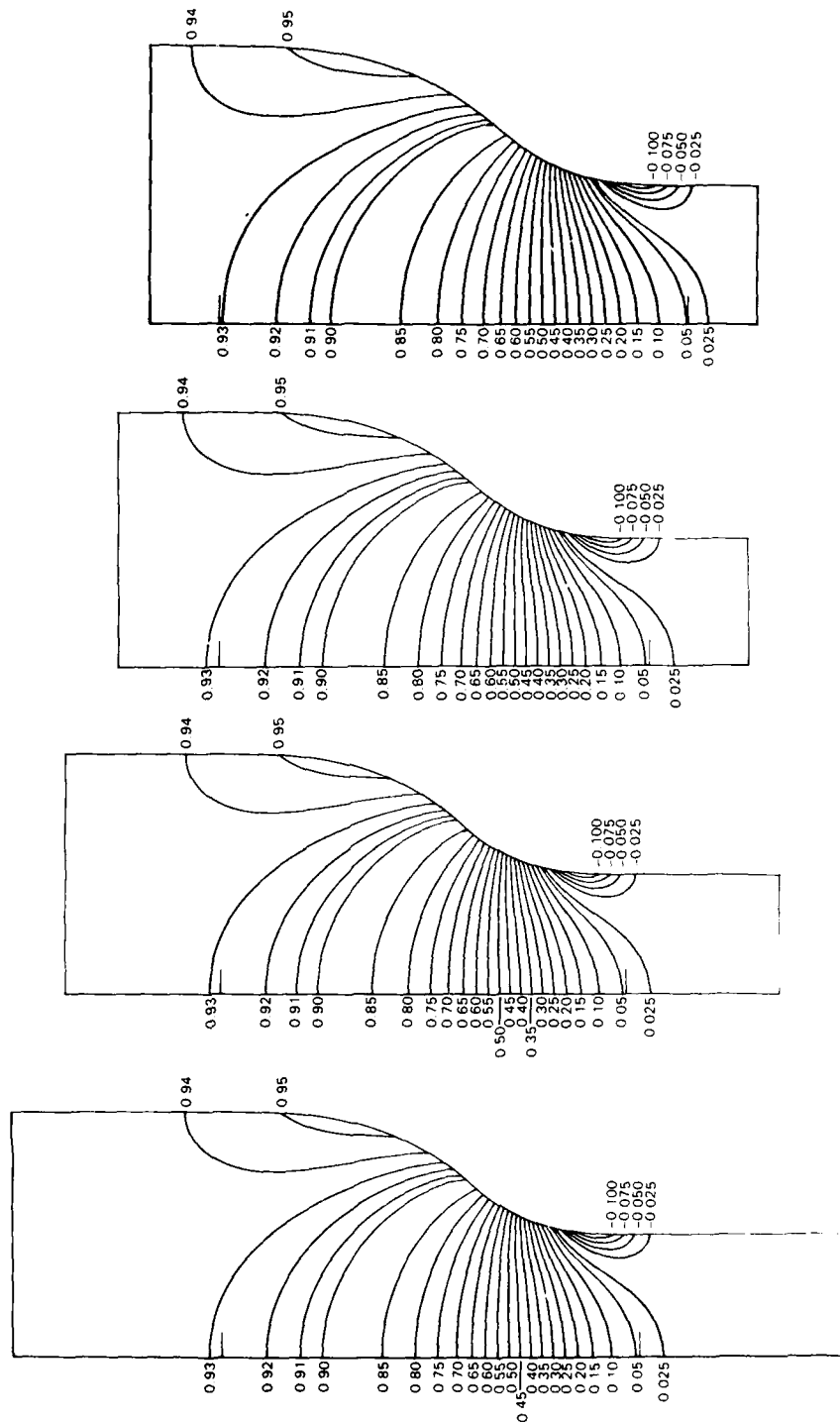


FIG. A2. CALCULATED C_p CONTOURS FOR DIFFERENT INLET/OUTLET EXTENSIONS X_e .
 (a) $X_e=0.125D$; (b) $X_e=0.225D$; (c) $X_e=0.325D$; (d) $X_e=0.425D$;
 ONLY THE CASE WITH $X_e=0.125$ HAS SIGNIFICANTLY DIFFERENT
 CONTOURS.

DISTRIBUTION

AUSTRALIA

Department of Defence

Defence Central

Chief Defence Scientist
Deputy Chief Defence Scientist (shared copy)
Superintendent, Science and Program Administration (shared copy)
Controller, External Relations, Projects and
Analytical Studies (shared copy)
Counsellor, Defence Science (London) (Doc Data Sheet Only)
Counsellor, Defence Science (Washington) (Doc Data Sheet Only)
S.A. to Thailand MRD (Doc Data Sheet Only)
S.A. to the DRC (Kuala Lumpur) (Doc Data Sheet Only)
OIC TRS, Defence Central Library
Document Exchange Centre, DISB (18 copies)
Joint Intelligence Organisation
Librarian H Block, Victoria Barracks, Melbourne

Aeronautical Research Laboratories

Director
Library
Superintendent - Aerodynamics
Divisional File - Aerodynamics
Author : J.H. Watmuff
N. Pollock
A. Goldman
B.D. Fairlie
J.M. Lopez

Materials Research Laboratories

Director/Library

Defence Research Centre

Library
Weapons Systems Research Laboratory
E.R.A. Landers, Aeroballistics

RAN Research Laboratory

Library

Navy Office

Navy Scientific Adviser (Doc Data Sheet Only)

Army Office

Scientific Adviser - Army (Doc Data Sheet Only)
Engineering Development Establishment, Library
Royal Military College Library

Universities

Kagawa University
Professor H.Ishikawa

NETHERLANDS

National Aerospace Laboratory (NLR), Library

NEW ZEALAND

Defence Scientific Establishment, Library

Universities

Canterbury
Library
Professor D.Stevenson, Mechanical Engineering

SWEDEN

Aeronautical Research Institute, Library

SWITZERLAND

F+W (Swiss Federal Aircraft Factory)

UNITED KINGDOM

Ministry of Defence, Research, Materials and Collaboration
CAARC, Secretary
Royal Aircraft Establishment
Bedford Library
Farnborough, Library
National Physical Laboratory, Library
National Engineering Laboratory, Library
British Library, Document Supply Centre
Aircraft Research Association, Library
Fulmer Research Institute Ltd, Research Director
Motor Industry Research Association, Director
Ricardo & Company Engineers (1927) Ltd, Manager
Rolls Royce Ltd, Aero Division Bristol, Library
British Aerospace
Kingston-upon-Thames, Library
Hatfield-Chester Division, Library
British Hovercraft Corporation Ltd, Library
Short Brothers Ltd, Technical Library

Universities

Bristol
Engineering Library

Cambridge
Library, Engineering Department
Whittle Library

London
Professor G.J.Hancock, Aero Engineering

Manchester
Professor, Applied Mathematics
Professor, N.Johannesen, Fluid Mechanics

Nottingham
Science Library

Southampton
Library

Liverpool
Fluid Mechanics Division, Dr.J.C.Gibbings

Strathclyde
Library

Cranfield Inst. of Technology
Library

Imperial College
Aeronautics Library

UNITED STATES OF AMERICA

NASA Scientific and Technical Information Facility
Boeing Company
Mr. W.E. Binz
Mr. J.C. McMillan
Kentex Research Library
Lockheed-California Company
Lockheed Missiles and Space Company
Lockheed Georgia
McDonnell Aircraft Company, Library

Universities and Colleges

Chicago
John Crerar Library

Florida
Aero Engineering Department
Professor D.C.Drucker

Johns Hopkins
Professor S.Corrin, Engineering

Iowa State
Dr. G.K. Serovy, Mechanical Engineering

Iowa
Professor R.I. Stephens

Princeton
Professor G.L. Mellor, Mechanics

Massachusetts Inst. of Tech.
MIT Libraries

Spares (10 copies)
Total (141 copies)

DOCUMENT CONTROL DATA

PAGE CLASSIFICATION
UNCLASSIFIED

PRIVACY MARKING

1a. AR NUMBER AR-004-496	1b. ESTABLISHMENT NUMBER ARL-AERO-R-171	2. DOCUMENT DATE AUGUST 1986	3. TASK NUMBER DST82/021
4. TITLE DESIGN OF A NEW CONTRACTION FOR THE ARL LOW SPEED WIND TUNNEL		5. SECURITY CLASSIFICATION (PLACE APPROPRIATE CLASSIFICATION IN BOX(S) IE. SECRET (S), CONF.(C) RESTRICTED (R), UNCLASSIFIED (U)). <input type="checkbox"/> U <input type="checkbox"/> U <input type="checkbox"/> U DOCUMENT TITLE ABSTRACT	6. NO. PAGES 36 7. NO. REFS. 14
8. AUTHOR(S) J.H. WATMUFF		9. DOWNGRADING/DELIMITING INSTRUCTIONS	
10. CORPORATE AUTHOR AND ADDRESS AERONAUTICAL RESEARCH LABORATORY P.O. BOX 4331, MELBOURNE VIC 3001		11. OFFICE/POSITION RESPONSIBLE FOR: SPONSOR _____ SECURITY _____ DOWNGRADING _____ APPROVAL _____	
12. SECONDARY DISTRIBUTION (OF THIS DOCUMENT)		Approved for Public Release	
OVERSEAS ENQUIRIES OUTSIDE STATED LIMITATIONS SHOULD BE REFERRED THROUGH DOCUMENT EXCHANGE CENTRE, DEFENCE INFORMATION SERVICES BRANCH, DEPARTMENT OF DEFENCE, CAMPBELL PARK, CANBERRA, ACT 2601			
13a. THIS DOCUMENT MAY BE ANNOUNCED IN CATALOGUES AND AWARENESS SERVICES AVAILABLE TO.... No limitations			
13b. CITATION FOR OTHER PURPOSES (IE. CASUAL ANNOUNCEMENT) MAY BE <input type="checkbox"/> UNRESTRICTED OR <input type="checkbox"/> AS FOR 13a.			
14. DESCRIPTORS Wind Tunnel Nozzles) Subsonic wind tunnels Flow distribution, <i>subsonic</i>		15. DRDA SUBJECT CATEGORIES 14020 01010	
16. ABSTRACT A numerical method is developed for the solution of Stokes's stream function. The method is applied to the existing Low Speed Wind Tunnel (LSWT) contraction shape. The calculated wall pressure coefficient distribution is compared to experimental measurements to test the approximation of axial symmetry made for the octagonal sections and for the effects of neglecting viscous forces. Reasonable agreement is obtained. The existing contraction is known to suffer from intermittent boundary layer separation near the entry caused by adverse pressure gradients. A new contraction shape is suggested that uses the contraction ratio of the existing			

PAGE CLASSIFICATION
UNCLASSIFIED

PRIVACY MARKING

THIS PAGE IS TO BE USED TO RECORD INFORMATION WHICH IS REQUIRED BY THE ESTABLISHMENT FOR ITS OWN USE BUT WHICH WILL NOT BE ADDED TO THE DISTIS DATA UNLESS SPECIFICALLY REQUESTED.

16. ABSTRACT (CONT.)

LSWT so that the new design can be installed within the existing LSWT in the form of an inner skin. The new design, which is about 10% longer than the existing contraction, has an adverse pressure gradient near the inlet which is about 1/5 of that of the existing contraction while the adverse pressure gradient near the exit is around the same value. It is expected that the reduced adverse pressure gradient near the entry will be small enough to allow the inlet boundary layer to remain attached thus leading to a substantial improvement to the working section flow quality. The new design could be installed upstream of the existing contraction to provide increased working section length.

17. IMPRINT

AERONAUTICAL RESEARCH LABORATORY, MELBOURNE

18. DOCUMENT SERIES AND NUMBER

Aerodynamics Report 171

19. COST CODE

55 6055

20. TYPE OF REPORT AND PERIOD COVERED

21. COMPUTER PROGRAMS USED

22. ESTABLISHMENT FILE REF.(S)

23. ADDITIONAL INFORMATION (AS REQUIRED)